Journal Name

COMMUNICATION

Charge Gradient-Induced On-Surface Growth of Ultralarge Single-crystalline Ag Nanomembranes for Long Surface Plasmon Propagation

Haili Qin,[†] Xiong Xiong,[†] Dongmin Wu,[†] Feng Zhang,[†] Dong Wang,[†] Xia Liu,[†] Wensheng Yang,[§]* and Jian Jin[†]*

A facile strategy for the fabrication of ultralarge (edge length > 50 μm), single-crystalline Ag nanomembranes is reported in this work. The Ag nanomembrane with atomically smooth surface demonstrates a much longer surface plasmonic propagation length as compared to vacuum-deposited polycrystalline Ag film, representing superior plasmonic property.

More and more research achievements have witnessed the importance of dimensionality of materials in determining their fundamental properties in addition to composition and arrangement of atoms, which has been significantly highlighted with graphene since 2004.[1] Inorganic nanomembranes (NMs), which possess single-crystalline structure with thickness of less than one hundred nanometers and with minimum lateral dimension at least three orders of magnitude larger than the thickness, have attracted widespread attention due to their unusual physical properties and extensive applications from sensors to electronics.[2] Fabrication of atom-thick two dimensional (2D) nanomaterials with intrinsically layered crystal structures of their bulk counterparts, such as metal chalcogenides, transition metal oxides, and metal hydroxides, have been effectively carried out through exfoliation technique, either mechanical or chemical exfoliation.[3] However, the preparation of inorganic NMs with nonlayered structure especially for most of metals and metal oxides is still underdeveloped and less of report due to lack of effective methods. The strong preference for three-dimensional (3D) close-packed structure of non-layered materials gives rise to weak driving force for 2D anisotropic growth.[4] A controlled strategy to inorganic NMs with nonlayered structure faces greatly challenging, which inspires the continuous and innovative exploration.

Noble metals (Ag, Au) with nanoscale dimensions are of great interest due to their unusual properties, such as optical, electronic, and catalytic properties, arising from their structural anisotropy, large surface areas and nearly perfect crystallinity.[5] What's more, noble metals with nanoscale structures enable light involved properties known as plasmonics, which are strongly size- and dimension-dependent.[6] Surface plasmon polaritons (SPPs) are intrinsically 2D electronmagnetic excitations those propagate along a metal-dielectric interface through hybridizing photo-electron waves.[7] Due to the unique hybrid character, SPPs can be developed to manipulate light below the optical diffraction limit and find their applications from subwavelength waveguides to photovoltaics.[8] Due to being confined to the near vicinity of the dielectric-metal interface, SPPs are often manipulated by surface patterning. In general, a patterned metal is often exploited to generate and manipulate SPPs where the precision of patterned structure and the dielectric properties related to surface roughness and homogeneity of the metals are the key factors in determining the performance of SPPs.[9] Therefore, to better generate SPPs, a rather smooth metal surface, meanwhile with high conductivity and low optical absorption is prerequisite to avoid SPP scattering and reduce propagation losses. Unfortunately, to date, the metal films examined for SPP properties are usually prepared by vacuum physical vapor deposition, which are inherently rough due to polycrystallinity with random grain orientation. The rather large surface roughness of vacuum-deposited metal films usually induce an extremely reduced propagation length.[4a,9c,9d] Therefore, single-crystalline novel metal films with precise patterned structure are highly desired. Although novel metal sheets with limited area have been prepared broadly via wet-chemistry method,[10] the synthesis of single-crystalline metal membranes with large areas applicable to plasmonic devices is still challenging and far less demonstrated.

We report in this work a facile strategy for the fabrication of ultralarge (edge length > 50 μm), single-crystalline Ag NMs via a charge gradient-induced on-surface process where positive-charged $Cu(OH)_2$ nanowire-haired copper mesh is used as template for directing the growth of Ag. Through such a wet-chemical process in mild condition, Ag NMs with uniform thickness (53 ± 3 nm) and atomically smooth surface are obtained. The investigation of SPPs on a patterned single-crystalline Ag NM with thickness of 50 nm demonstrates a much longer propagation length as compared to on a patterned vacuum-deposited polycrystalline film, representing superior plasmonic property.

As schematically shown in Figure 1a, $Cu(OH)_2$ nanowire-haired copper mesh was firstly prepared via oxidation reaction in an alkaline aqueous solution containing $(NH_4)_2S_2O_8$ according to our previous report.[11] Scanning electron microscopy (SEM) images show that the whole framework of copper mesh (Figure 1b) is twined uniformly and densely by hairy nanowires after oxidation (Figure 1c). The nanowires growing vertically along the mesh walls have a length of 10-15 μm and diameters within the range of 200-

500 nm. The composition of the nanowires is orthorhombic-phase $Cu(OH)_2$ crystal (JCPDS: No. 13-0420) as proved by X-ray diffraction (XRD) spectrum (Figure S1b). The nanowire-haired copper mesh behaves superhydrophilic property with quickly spreading and penetrating process of water droplet recorded by a high-speed camera system (Figure S1d). In other word, water can fully wet and infiltrate into the inner of nanowire network. It assures the complete oxidation-reduction reaction between the reactant in aqueous solution and reactant on copper mesh.
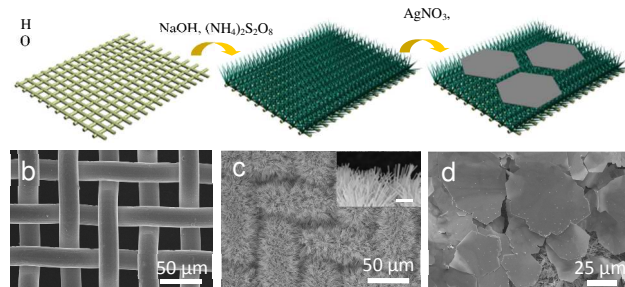
Figure 1. (a) Schematic illustration of the synthesis of Ag NMs on $Cu(OH)_2$ nanowire-haired copper mesh. SEM images of (b) the original copper mesh with a mesh number of 500, (c) $Cu(OH)_2$ nanowire-haired copper mesh (inset: enlarged cross-section SEM image of the nanowire-haired copper mesh, scale bar: 5 μm), and (d) Ag NMs grown on the surface of nanowire-haired copper mesh.

To grow Ag NMs, a certain amount of $AgNO_3$ and ethylene glycol is added into the aqueous solution where a piece of nanowire-haired inorganic membrane (1 cm × 1 cm) is immersed into the solution beforehand. Under the reduction of Cu skeleton of the mesh membrane, Ag^+ is reduced to Ag^0 and the whole reaction is preceded at room temperature. After one-day reaction, the surface of the mesh membrane turns into white color, indicating the generation of Ag and the aqueous solution becomes to be light blue due to the oxidation of Cu. As can be seen from Figure 1d, the surface of mesh membrane is covered by a large amount of Ag NMs with an average edge length of 30-70 μm. The obtained Ag NMs could be easily peeled off from the mesh membrane by an ultrasonic treatment.
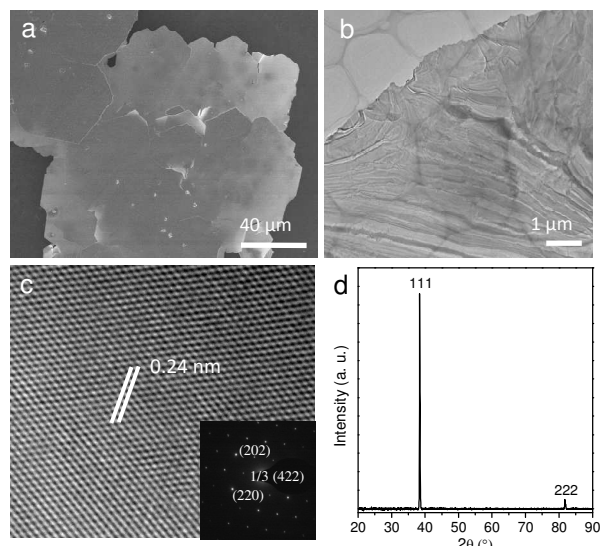
Figure 2. Morphology and structure characterization of Ag NMs. Representative (a) SEM and (b) TEM images of Ag NMs. (c)

HRTEM image of a Ag NM and (inset) SAED pattern. (d) XRD pattern of Ag NMs.

Figure 2a and 2b show SEM and transmittance electron microscopy (TEM) images of the Ag NMs, indicating the presence of well-defined, large area 2D products with few particles or impurities within the field. A high-resolution TEM (HRTEM) image taken from the Ag nanomembrane in Figure 2b reveals it to be single-crystalline, and the lattice parameter can be calculated to be 0.24 nm (Figure 2c).[10e] The corresponding selected-area electron diffraction (SAED) pattern obviously proves the single crystalline property of Ag membrane, and the hexagonal diffraction spots prove it to be highly (111)-oriented (Figure 2c, inset).[10c,10f] The set of spots of 1/3{422} reflection, usually forbidden in a face-centered cubic (fcc) lattice, indicates that the surfaces of Ag NMs are atomically flat.[4a] In the XRD spectrum, the overwhelmingly strong diffraction peak at $2\theta = 38.4°$ and its secondary diffraction peak at $2\theta = 81.7°$ are assigned to (111) reflection of the fcc structure of metallic Ag. These results reveal a preferred orientation of Ag NMs in the (111) direction. The thickness of Ag membranes could be statistical calculated to be 53 ± 3 nm by utilizing an optical imaging method combined with image analysis software (Figure S2 and Table S1 and detail description herein).[4a,12]
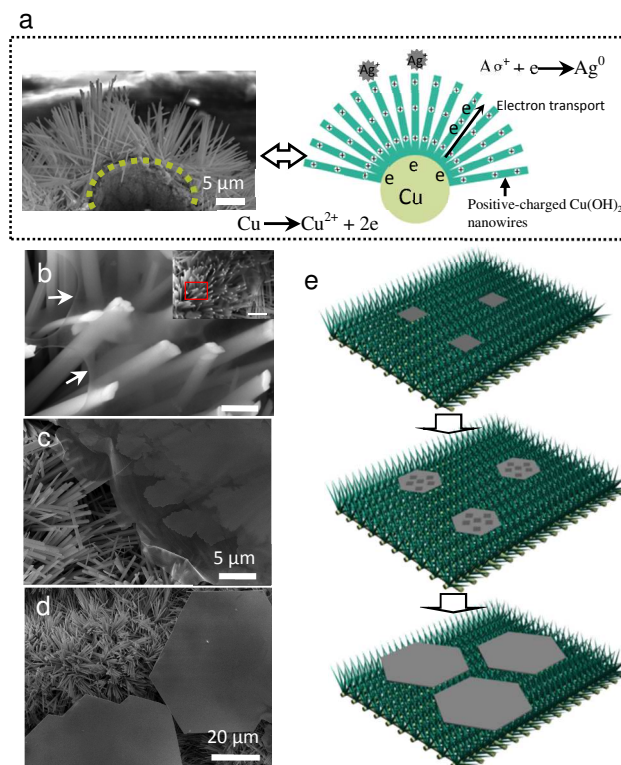
Figure 3. Formation process of Ag NMs on the $Cu(OH)_2$ nanowire-haired copper mesh. (a) Left: cross-section SEM image of $Cu(OH)_2$ nanowire-haired copper mesh. The area marked by a dashed circle indicates the Cu skeleton in the copper mesh; right: a schematic figure for the $Cu(OH)_2$ nanowire-haired copper mesh with positive charges distributed along $Cu(OH)_2$ nanowire and the redox reaction of Ag^+ into Ag^0 occurs. SEM images of the intermediate product along different reaction time: (b) 0.5 h (inset: low-magnification SEM image, scale bar, 5 μm), (c) 1 h, (d) 8 h. (e) Schematic illustration of the time-dependent morphology evolution process for the formation of Ag NMs corresponding b-d.

As for the growth mechanism of Ag NMs on the nanowire-haired mesh membrane, we propose a process of positive-charge gradient induced redox reaction on nanowire surface. Basically, Ag^+ could be reduced by the copper skeleton of mesh membrane due to lower reduction potential of Ag than Cu. But what is special in this work is that the formation of Ag NMs only occurs on the surface of $Cu(OH)_2$ nanowires. Two functions are supposed to play key roles on the growth of Ag nanostructures. One of them is ascribed to the positive-charge gradient of the nanowire-haired mesh surface. It has been tested that the $Cu(OH)_2$ nanowires grown on mesh surface is positively charged with the zeta potential of 14.2 mV (Figure S3). As can been seen that the growth of $Cu(OH)_2$ nanowires on copper mesh is divergent around the mesh skeleton, like the structure of sea urchins (Figure 3a). The nearer the nanowires get to the Cu skeleton, the denser they are. The packing density gradient of nanowires also gives rise to a positive-charge gradient (e.g. positive-charge number per unit area). This means that the intensity of positive potential of copper mesh decreases along the direction of nanowires growth. Due to electrostatic repulsion, the positive-charged silver ions are difficult to enter into the inner of the nanowire walls. Therefore, the silver ions closer to the exterior of the nanowire walls, that is the outer pointed end of nanowire, are easier to be reduced. During this process, $Cu(OH)_2$ nanowires act as electron transporters to transport the electrons of Cu skeleton to the outer pointed end of nanowires where the reduction of silver ions occurs. 1D nanostructures of metal hydroxides grown on conductive substrate have been proved to act as effective electron mediators/transporters during electrochemical processes.[13] The function of positive-charge gradient and thus electrostatic repulsion of silver ions and nanowire walls has been verified by a control experiment where chloroauric acid ($HAuCl_4$) is used as source material instead of $AgNO_3$. Different from positive-charged silver ion, the $AuCl_4^-$ is negative-charged. In this case, $AuCl_4^-$ could be also reduced to Au^0 and Au nanoparticles are formed (Figure S4). However, different from what we observed in the case of Ag, it is found that the Au nanoparticles are produced around the nanowire surfaces but not on nanowire surfaces. It is attributed to the electrostatic attraction between nanowires and $AuCl_4^-$ ions. Another important role during the formation of Ag NMs is ascribed to ethylene glycol added into the solution. It has been well-known that ethylene glycol as a kind of polyols can be used as stabilizer and shape-controlling agent in the synthesis of nanostructures of noble metals, especially for 2D nanomaterials. The introduction of ethylene glycol play a crucial role in controlling the ratio of growth rates for different crystallographic planes and have a profound impact on the final shape of the metal nanostructures.[14] In a control experiment, Ag with dendritic structures instead of Ag NMs are produced only in this system when no ethylene glycol is added in the solution (Figure S5). It is worth to note that ethylene glycol is chemical stable and could not be reduced under our experimental condition. The time-dependent morphology evolution has been monitored by SEM observation and the corresponding scheme is also drawn (Figure 3b-e). At the initial stage, ultrathin and transparent Ag films with irregular edges are formed and propped up by nanowires as marked by arrows and can be seen clearly (Figure 3b). With the reaction going on, the untrathin films grow further into larger ones and become thicker and thicker driven by both Ostwald ripening and oriented attachment processes (Figure 3c).

Due to the large area and smooth surface of our Ag NMs, it is important to investigate their plasmonic properties. By using SEM and cathodluminescence (CL) spectroscopy, the propagation distance of SPPs propagating along Ag surface is measured. To generate SPPs, focused-ion-beam (FIB) milling was employed to fabricate a regular grating pattern (periodicity width: 700 nm, grid width: 500 nm, grid length: 8 μm) on the membrane. What deserves to be mentioned is that it is the first time to fabricate patterned structures on a single-crystalline Ag NM. Figure 4a and 4b are low- and high-magnification SEM images of a patterned single-crystalline Ag membrane. The smoothness of the single-crystalline Ag membrane and grid structure with precise and sharp boundaries can be observed. To better understand the improved plasmonic property of our single-crystalline Ag NMs, a vacuum-deposited and patterned Ag film with same thickness and similar pattern structure as the single-crystalline Ag NM was fabricated by combing magnetron sputtering with FIB milling. As shown in Figure 4c and 4d, the surface of the deposited polycrystalline Ag film is rather rough, especially on the widened pattern grids due to the grain boudaries during the FIB milling process as compared with the Ag NM. The flatnesses of the single-crystalline Ag membrane and the deposited Ag film were further analyzed with atomic force microscope (AFM) (Figure S6a and 6b). The root mean square (RMS) roughness for the Ag membrane is quantified to be 1.28 nm over 800 nm × 800 nm region, indicating an atomically smooth surface. As for the deposited Ag film, the RMS roughness is as high as 15.5 nm, a representative value for most polycrystalline Ag films.
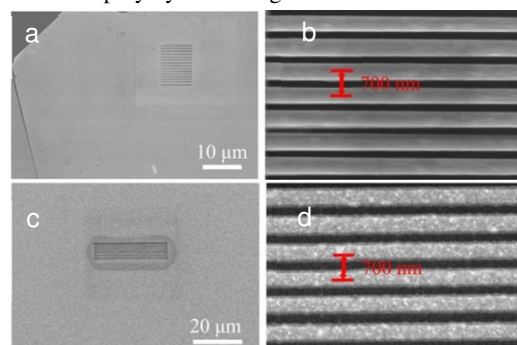
Figure 4. SEM images of Ag NM (a) and deposited Ag film (c) patterned with regular gratings. Enlarged SEM images of patterned grid on the Ag NM (b) and deposited Ag film (d).

The SPP propagation lengths of the two types of Ag films were then measured. As schematically shown in Figure 5, an electron beam from FEI SEM with a diameter of around 5 nm was used to excite SPPs of Ag membrane at a position micrometer away from the edge of the pattern structures.[9d] In principle, the plasmons are propagated along the Ag surface and decayed exponentially with distance from the surface. Due to the interaction with surface patterns, SPPs could be coupled to the free space photon modes when striking the gratings, which was collected by an optical microscope placed over the sample. The spectra of scattered light obtained changing the distance between grating and excitation spot were measured, from which we could extract the function between the propagation length of SPP and optical wavelength.[15] The resulting SPP propagation lengths over the detected wavelength coverage (450-600 nm) for the two types of Ag film are shown in Figure 5. The results clearly show that the propagation length on a single-crystalline Ag NM is much longer than on the deposited Ag film, exhibiting an average 500% improvement. The theoretical propagation lengths on Ag can be calculated by assuming the surface of Ag film with zero roughness and the SPPs damping only by Ohmic losses as shown in the figure too. The SPP results demonstrate that our single-crystalline Ag NMs possess high quality and superior SPP property, indicating their great promise for applications in plasmonic devices.
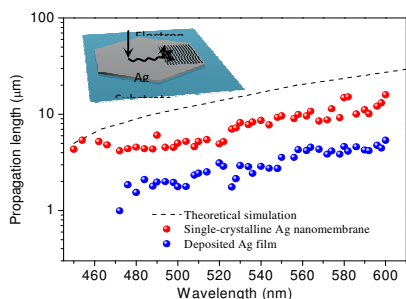
Figure 5. SPP propagation lengths on the Ag NM and deposited Ag film. The dashed line is the predicted propagation length using the dielectric constant of single-crystalline sample when assuming only Ohmic losses and no roughness, inset: schematic diagram of the experiment setup for generating SPPs on a Ag NM.

Conclusions

In summary, we have successfully prepared ultralarge (edge length > 50 μm) single-crystalline Ag NMs in a distinctive system where a positive-charged $Cu(OH)_2$ nanowire-haired copper mesh was utilized as template. Due to the atomically smooth surfaces and large areas, the produced Ag NMs exhibit superior surface plasmonic properties as compared to vacuum-deposited polycrystalline film. The on-surface growth of 2D nanomaterials induced by positive-charge gradient has demonstrated its effectiveness and provides a powerful alternative route for the preparation of 2D nonlayered nanomaterials with a device-processible scale.

Notes and references

[†]Nano-Bionics Division and *i*-Lab, Suzhou Institute of Nano-Tech and Nano-Bionics, Chinese Academy of Sciences, Suzhou 215123, China.
[§]State Key Laboratory of Supramolecular Structure and Materials, College of Chemistry, Jilin University, Changchun 130012, China.

Corresponding Author

wsyang@jlu.edu.cn; jjin2009@sinano.ac.cn

Acknowledgment

1 (a) R. F. Service, *Science,* 2009, **324**, 875; (b) K. S. Novoselov, Z. Jiang, Y. Zhang, S. V. Morozov, H. L. Stormer, U. Zeitler, J. C. Maan, Boebinger, G. S.; Kim, P.; Geim, A. K. *Science,* **2007**, *315*, 1379; (c) A. K. Geim, *Science,* 2009, **324**, 1530; (d) J. S. Bunch, A. M. vander Zande, S. S. Verbridge, I. W. Frank, D. M. Tanenbaum, J. M. Parpia, Craighead, H. G.; McEuen, P. L. *Science,* **2007**, *315*, 490; (e) Lee, C.; X. Wei, J. W. Kysar, J. Hone, *Science,* 2008, *321*, 385.
2 (a) Y. Liu, X. Dong, P. Chen, *Chem. Soc. Rev.,* 2012, **41**, 2283; (b) F. K.erkins, A. L.riedman, E. Cobas, P. M. Campbell, G. G. Jernigan, B. T. Jonker, *Nano Lett.,* 2013, **13**, 668; (c) Q. H. Wang, K. Kalantar-Zadeh, A. Kis, J. N. Coleman, M. S. Strano, *Nat. Nanotech.,* 2012, **7**, 699; (d) H. Li, Z. Song, X. Zhang, Y. Huang, S. Li, Y. Mao, H. J. Ploehn, Y. Bao, M. Yu, *Science,* 2013, **342**, 95; (e) H. W. Kim, H. W.

Yoon, S. M. Yoon, B. M. Yoon, B. K. Ahn, Y. H. Cho, H. J. Shin, H. Yang, U. Paik, S. Kwon, J. Y. Choi, H. B. Park, *Science,* 2013, **342**, 91; (f) Y. Han, Z. Xu, C. Gao, *Adv. Mater.,* 2013, **23**, 3693; (g) H. Li, Y. Huang, Y. Mao, W. L. Xu, H. J. Ploehn, M. Yu, *Chem. Commun.,* 2014, **50**, 9849.
3 (a) K. S. Novoselov, A. K.eim, S. V.orozov, D. Jiang, Y. Zhang, S. V. Dubonos, I. V. Grigorieva, A. A. Firsov, *Science,* 2004, **306**, 666; (b) J. N. Coleman, M. Lotya, A. O'Neill, S. D. Bergin, P. J. King, U. Khan, K. Young, A. Gaucher, S. De, R. J. Smith, I. V. Shvets, S. K. Arora, G. Stanton, H. Y. Kim, K. Lee, G. T. Kim, G. S. Duesberg, T. Hallam, J. J. Boland, J. J. Wang, J. F. Donegan, J. C. Grunlan, G. Moriarty, A. Shmeliov, R. J. Nicholls, J. M. Perkins, E. M. Grieveson, K. Theuwissen, D. W. McComb, P. D. Nellist, V. Nicolosi, *Science,* 2011, **331**, 568; (c) M. R. Lukatskaya, O. Mashtalir, C. E. Ren, Y. Dall'Agnese, P. Rozier, P. L. Taberna, M. Naguib, P. Simon, M. W. Barsoum, Y. Gogotsi, *Science,* 2013, **341**, 1502; (d) R. Ma, Z. Liu, K. Takada, N. Iyi, Y. Bando, T. Sasaki, *J. Am. Chem. Soc.,* 2007, **129**, 5257.
4 (a) H. L. Qin, D. Wang, Z. L. Huang, D. M. Wu, Z. C. Zeng, B. Ren, K. Xu, J. Jin, *J. Am. Chem. Soc.,* 2013, **135**, 12544; (b) Z. Tang, Z. Zhang, Y. Wang, S. C. Glotzer, N. A. Kotov, *Science,* 2006, **314**, 274; (c) C. Schliehe, B. H. Juarez, M. Pelletier, S. Jander, D. Greshnykh, M. Nagel, A. Meyer, S. Foerster, A. Kornowski, C. Klinke, H. Weller, *Science,* 2010, **329**, 550; (d) X. Zhang, J. Zhang, J. Zhao, B. Pan, M. Kong, J. Chen, Y. Xie, *J. Am. Chem. Soc.,* 2012, **134**, 11908.
5 (a) L. Hu, H. S. Kim, J. Y. Lee, P. Peumans, Y. Cui, *ACS Nano,* 2010, **4**, 2955; (b) M. C. Daniel, D. Astruc, *Chem. Rev.,* 2004, **104**, 293; (c) P. K. Jain, X. Huang, I. H. El-Sayed, M. A. El-Sayed, *Acc. Chem. Res.,* 2008, **41**, 1578.
6 (a) M. Rycenga, C. M. Cobley, J. Zeng, W. Li, C. H. Moran, Q. Zhang, D. Qin, Y. Xia, *Chem. Rev.,* 2011, **111**, 3669; (b) R. Jin, Y. Cao, C. A. Mirkin, K. L. Kelly, G. C. Schatz, J. G. Zheng, *Science,* 2001, **294**, 1901; (c) Z. Huo, C. Tsung, W. Huang, X. Zhang, P. Yang, *Nano Lett.,* 2008, **8**, 2041.
7 H. Rather, *Surface plasmon* Springer-Verlag, Berlin, 1998.
8 (a) R. F. Oulton, V. J. Sorger, D. A. Genov, D. F. P. Pile, X. Zhang, *Nat. Photon.,* 2008, **2**, 496; (b) P. Mühlschlegel, H. J. Eisler, O. J. F. Martin, B. Hecht, D. W. Pohl, *Science,* 2005, **308**, 1607; (c) J. S. Huang, V. Callegari, P. Geisler, C. Brüning, J. Kern, J. C. Prangsma, X. Wu, T. Feichtner, J. Ziegler, P. Weinmann, M. Kamp, A. Forchel, P. Biagioni, U. Sennhauser, B. Hecht, *Nat. Commun.,* 2010, **1**, 150; (d) S. I. Bozhevolnyi, V. S. Volkov, E. Devaux, J. Y. Laluet, T. W. Ebbesen, *Nature,* 2006, **440**, 508.
9 (a) W. L. Barnes, A. Dereux, T. W. Ebbesen, *Nature,* 2003, **424**, 824; (b) P. Nagpal, N. C. Lindquist, S. H. Oh, D. J. Norris, *Science,* 2009, **325**, 594; (c) J. H. Park, P. Ambwani, M. Manno, N. C. Lindquist, P. Nagpal, S. H. Oh, C. Leighton, D. J. Norris, *Adv. Mater.,* 2012, **24**, 3988; (d) J. T. van Wijngaarden, E. Verhagen, A. Polman, C. E. Ross, H. J. Lezec, H. A. Atwater, *Appl. Phys. Lett.,* 2006, **88**, 221111.
10 (a) R. Jin, Y. C. Cao, E. Hao, G. S. Metraux, G. C. Schatz, C. A. Mirkin, *Nature,* 2003, **425**, 487; (b) J. E. Millstone, S. Park, K. L. Shuford, L. Qin, G. C. Schatz, C. A. Mirkin, *J. Am. Chem. Soc.,* 2005, **127**, 5312; (c) J. Zeng, X. Xia, M. Rycenga, P. Henneghan, Q. Li, Y. Xia, *Angew. Chem. Int. Ed.,* 2011, **50**, 244; (d) A. Courty, A. I. Henry, N. Goubet, M. P. Pileni, *Nat. Mater.,* 2007, **6**, 900; (e) Z. Deng, M. Mansuipur, A. J. Muscat, *J. Phys. Chem. C,* 2009, **113**, 867; (f) Q. Zhang, Y. Hu, S. Guo, J. Goebl, Y. Yin, *Nano Lett.,* 2010, **10**, 5037.
11 F. Zhang, W. B. Zhang, Z. Shi, D. Wang, J. Jin, L. Jiang, *Adv. Mater.* 2013, **25**, 4192.
12 H. Li, G. Lu, Z. Yin, Q. He, H. Li, Q. Zhang, H. Zhang, *Small* 2012, **8**, 682.
13 (a) S. Zhou, X. Feng, H. Shi, J. Chen, F. Zhang, W. Song, *Sens. Actuators B: Chem.,* 2013, **177**, 445; (b) J. Jiang, J. Liu, R. Ding, J. Zhu, Y. Li, A. Hu, X. Li, X. Huang, *ACS Appl. Mater. Interfaces,* 2011, **3**, 99.
14 (a) C. Li, W. Cai, B. Cao, F. Sun, Y. Li, C. Kan, L. Zhang, *Adv. Funct. Mater.,* 2006, **16**, 83; (b) S. Nootchanat, C. Thammacharoen, B. Lohwongwatana, S. Ekgasit, *RSC Adv.,* 2013, **3**, 3707; (c) H. Huang, X. Yang, *Biomacromolecules,* 2004, **5**, 2340; (d) H. Yue, Y. Zhao, X. Ma, J. Gong, *Chem. Soc. Rev.,* 2012, **41**, 4218.
15 J. A. Dionne, L. A. Sweatlock, H. A. Atwater, A. Polman, *Phys. Rev. B,* 2005, **72**, 075405.